



ELSEVIER

Available online at www.sciencedirect.com

SCIENCE @ DIRECT®

Journal of Volcanology and Geothermal Research xx (2005) xxx–xxx

Journal of volcanology
and geothermal researchwww.elsevier.com/locate/jvolgeores

The 12.1 ka Middle Toluca Pumice: A dacitic Plinian–subplinian eruption of Nevado de Toluca in Central Mexico

J.L. Arce^{a,*}, K.E. Cervantes^b, J.L. Macías^c, J.C. Mora^c

^a*Instituto de Geología, UNAM Coyoacán 04510, México, DF, Mexico*

^b*Posgrado en Ciencias de la Tierra, Instituto de Geología, UNAM Coyoacán 04510, México, DF, Mexico*

^c*Departamento de Vulcanología, Instituto de Geofísica, UNAM Coyoacán 04510, México, DF, Mexico*

Received 17 March 2004; received in revised form 15 March 2005; accepted 31 March 2005

Abstract

The Nevado de Toluca volcano erupted explosively approximately 12.1 ka ago, producing a Plinian–subplinian eruption that deposited the Middle Toluca Pumice (MTP). The MTP consists of white and gray juvenile pumice, gray dense juvenile lapilli, and red altered lithic lapilli. The pumice is dacitic (63.54–65.06 wt.% SiO₂) with phenocrysts of plagioclase > orthopyroxene > hornblende ± ilmenite and titanomagnetite, and biotite xenocrysts set in a groundmass of rhyolitic glass (70–71 wt.% SiO₂). The MTP has a dispersal axis to the ESE covering an area of 92 km², with a minimum volume of 1.8 km³ (DRE). Stratigraphic relations, grain size, componentry, and vesicularity analyses suggest that the eruption occurred in five major phases: (1) an opening magmatic phase that generated a 20-km-high Plinian column dispersed to the SE; (2) a hydromagmatic explosion followed with the establishment of a subplinian eruptive column (18–19 km high) dispersed tephra to the SE and gradually waned; (3) hydromagmatic explosions emplaced dilute pyroclastic density currents followed by the formation of an eruptive column of unknown height; (4) immediately after, a new magmatic explosion established another eruptive column; and (5) the collapse of the latter column generated two pumiceous pyroclastic density currents that were fully dilute proximally, but transformed into two granular-fluid pyroclastic currents that traveled 19 km from the source. © 2005 Elsevier B.V. All rights reserved.

Keywords: late Pleistocene; Plinian–subplinian eruption; Nevado de Toluca; Central Mexico

1. Introduction

Plinian and subplinian eruptions are characterized by the formation of convective eruption columns;

however, some differences exist between them in terms of magnitude and intensity (Cioni et al., 2000). For example, Plinian eruptions develop steady, sustained, convective columns, whereas subplinian eruptions tend to generate unsteady, convective columns, a feature which is recorded in the characteristics of their deposits (Bursik, 1993; Cioni et al., 2000, 2003). Deposits produced by subplinian eruptions

* Corresponding author. Tel.: +52 56224299x108; fax: 52 56224289.

E-mail address: jlance@geologia.unam.mx (J.L. Arce).

commonly show grain-size stratification and are frequently interlayered with pyroclastic surges (Sieh and Bursik, 1986; Cioni et al., 2003), which reflect the unsteady state of the eruptive column. The 12.1 ka Middle Toluca Pumice (MTP) pyroclastic sequence of Nevado de Toluca volcano represents another case to better understand these variations. The MTP fall layers do not show the classic stratified nature of the subplinian fall deposits; however, according to grain-size characteristics, this sequence lies between Plinian- and subplinian-type eruptions (Pyle, 1989). Therefore, in this paper, we describe the MTP sequence as the product of a Plinian–subplinian eruption. It is compared with other well-studied Plinian eruptions of Nevado de Toluca volcano.

Nevado de Toluca volcano ($19^{\circ}06'30''\text{N}$; $99^{\circ}45'30''\text{W}$; 4680 m asl), located 80 km WSW from Mexico City, is part of the Trans-Mexican Volcanic Belt (TMVB) (Fig. 1A and B). The volcano erupted 3300 years ago (Macías et al., 1997) and is considered a quiescent active volcano. During the

last 40,000 years, it has undergone at least five dome destruction and collapse eruptions (at 37, 32, 28, 26, and 13 ka) and four Plinian eruptions (at 36, 21.7, 12.1, and 10.5 ka) (García-Palomo et al., 2002; Arce et al., 2003; Capra et al., in press); hence a future eruption might be of Plinian type. The past Plinian products of the volcano have had a generally ENE dispersal axis (Bloomfield et al., 1977; Arce et al., 2003; Capra et al., in press). In this direction lie the metropolitan areas of Toluca and Mexico cities, where more than 25 million people live (INEGI, 1995). These two areas have undergone substantial economic development during the last few decades with the establishment of high-tech factories, an international airport, and major national highways that connect this region with other important cities (e.g., Guadalajara, Monterrey, and Colima). To better understand the potential hazards posed by Nevado de Toluca, detailed studies of its explosive events and dome collapses are needed. Previous work has focused on the most recent Plinian event, the

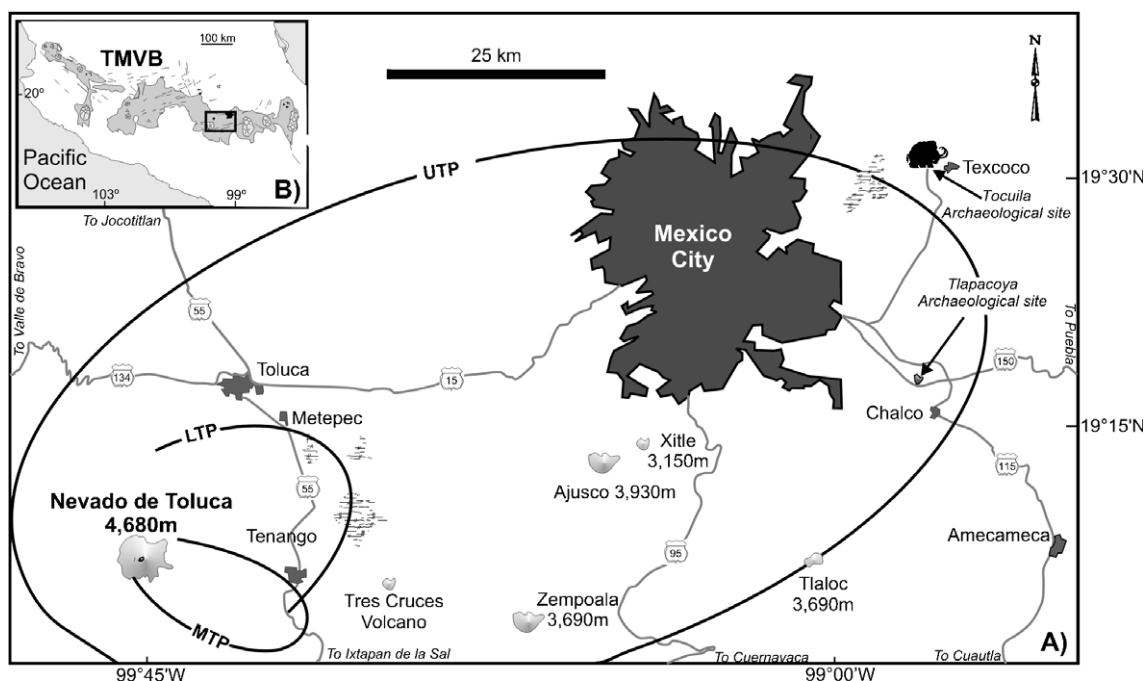


Fig. 1. (A) Location of Nevado de Toluca volcano showing the 10-cm isopachs of the three most recent Plinian eruptions of the volcano. UTP=Upper Toluca Pumice; MTP=Middle Toluca Pumice; LTP=Lower Toluca Pumice deposits. (B) Location of Nevado de Toluca volcano within the Trans-Mexican Volcanic Belt (TMVB) in Central Mexico.

Upper Toluca Pumice (Arce et al., 2003). Here, we reconstruct the eruptive sequence of the penultimate event by determining the distribution of the deposits, total volume, column height, and mass discharge rate, as well as the eruption dynamics.

Macías et al. (1997) proposed that the deposits consist of an alternating sequence of pyroclastic fall, surge, and flow layers, informally grouping them as the White Pumice Flow deposit. Recently, Cervantes (2001), García-Palomo et al. (2002), and Arce et al. (2003) defined stratigraphic relations with the underlying and overlying units, and dated the deposit at 12.1 ka. In this paper, we propose the informal name of Middle Toluca Pumice (MTP) to describe this sequence because it lies between the Lower Toluca Pumice (21.7 ka) and the Upper Toluca Pumice (10.5 ka) (Bloomfield and Valastro, 1974, 1977; Bloomfield et al., 1977; Arce et al., 2003; Capra et al., in press).

2. Age of the MTP deposit

A paleosol underlying the MTP was dated at $26,275 \pm 1210 / -150$ years BP (Macías et al.,

1997). Two samples of charred logs in the MTP pyroclastic flow have yielded ages of $12,415 \pm 290 / -280$, and $12,040 \pm 92$ years BP (Table 1) (García-Palomo et al., 2002), which are interpreted to date the MTP eruption. Another charred log found within the pyroclastic flow of the MTP deposit at site 32 (Fig. 2) yielded an age of $12,515 \pm 95$ years BP (Table 1). The MTP deposit has been correlated with the so-called “Lower Almoloya Tephra” near Almoloya village (Newton and Metcalfe, 1999), where an underlying clay layer, rich in organic material, has been dated at $12,400 \pm 60$ years BP (Table 1) and would represent a maximum age for the MTP. At site 161, the MTP underlies a paleosol dated at $11,595 \pm 180$ years BP. On the other hand, the 10.5 ka Upper Toluca Pumice (UTP) contains two charred logs in pyroclastic flow deposits that yielded ages of 12,120 and 12,195 years BP, older than the underlying paleosol (Arce et al., 2003). These latter authors interpreted the charcoal fragments as having been derived from the MTP by erosion associated with the UTP pyroclastic flows, and thus their ages yield an approximate age of the MTP eruption.

Table 1
Radiocarbon dates of the Middle Toluca Pumice and related deposits of Nevado de Toluca volcano

Sample	Laboratory	Conventional age (years BP)	Calibrated age range $\pm 1\sigma$ (BP)	Material dated	Latitude N	Longitude W	Reference
NT9570-CAR	WW1876	$12,090 \pm 40$	15,076 (14,096) 13,851	Charcoal within UTP pyroclastic flow horizon	$19^{\circ}17'30''$	$99^{\circ}21'$	Macías et al. (1997)
KBC-35	Tx-1655	9080 ± 100	10,360 (10,222) 10,186	Humic clayey layer, Sierra de Las Cruces	$19^{\circ}19'30''$	$99^{\circ}18'$	Bloomfield and Valastro (1977)
NT97200	A-9781	$12,040 \pm 90$	14,124 (14,079) 13,838	Charcoal in MTP deposit			García-Palomo et al. (2002)
NT97161-B	A-11161	$12,120 \pm 85$	15,209 (14,133) 14,089	Charcoal within UTP pyroclastic flow horizon	$19^{\circ}04'$	$99^{\circ}39'$	Arce et al. (2003)
NT97161-A	A-11160	$12,195 \pm 103$	15,128 (14,106) 13,855	Charcoal within UTP pyroclastic flow horizon	$19^{\circ}04'$	$99^{\circ}39'$	Arce et al. (2003)
NT96161	A-9472	$12,415 \pm 285$	15,443 (14,343) 14,106	Charcoal in MTP deposit	$19^{\circ}04'$	$99^{\circ}39'$	García-Palomo et al. (2002)
LAT	Beta-94129	$12,400 \pm 60$	14,336, 12,387	Organic clay	$19^{\circ}09'$	$99^{\circ}31'$	Newton and Metcalfe (1999)
NT9545	A-8485	$26,275 \pm 1210 / -150$		Paleosol below MTP deposit	$19^{\circ}03'$	$99^{\circ}39'$	Macías et al. (1997)
PBAF-31	A-11332	$38,400 \pm 1300$		Charcoal inside pink block-and-ash flow deposit, found below MTP	$19^{\circ}04'$	$99^{\circ}39'$	Cervantes (2001)

Calibrated ages based on CALIB (Stuiver and Reimer, 1993, version 4.1) and calibration data set by Stuiver et al. (1998).

In summary, the dates obtained from charcoal samples in the MTP vary from $12,040 \pm 92$ to $12,515 \pm 95$ years BP, and we consider the most probable age of the eruption to be $\sim 12,100$ years BP.

3. Stratigraphy of the deposit

The MTP crops out on the ESE slopes of the volcano (Fig. 2). A composite stratigraphic column of the MTP (Fig. 3) was constructed from 71 detailed stratigraphic sections, and we were able to correlate and characterize each fall layer, flow, and surge deposits that comprise the MTP succession (Fig. 4).

The main components of the MTP, in order of abundance are: white pumice, dense juvenile lithics, red altered lithics, gray pumice, crystals, and glass. The white pumice is finely vesiculated, and contains phenocrysts of plagioclase, orthopyroxene, hornblende, and biotite. We now describe the stratigraphic succession from the base upwards, with the granulometric parameters of Inman (1952).

4. Layer C1

Layer C1 overlies a brown paleosol developed at the top of an older ignimbrite (e.g., site 73; Fig. 5). At other localities along the Cieneguilla gully, it rests

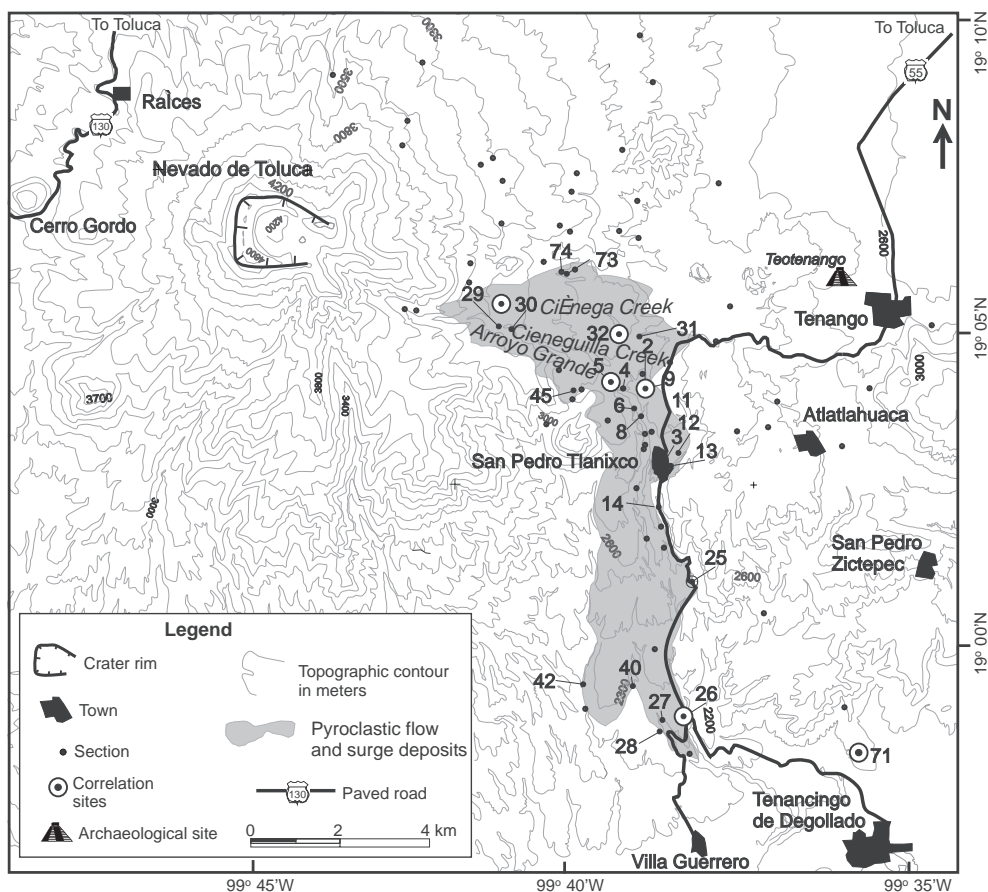


Fig. 2. Topographic map of the studied area, where many of the stratigraphic sections are located. Numbers indicate sites mentioned in the text. Large circles represent sections shown in Fig. 4. The shaded area shows the distribution of the pyroclastic flow deposits (FB1 and FB2) of the MTP sequence. Note that the emplacement of the pyroclastic flows was controlled by the topography of Arroyo Grande gully.

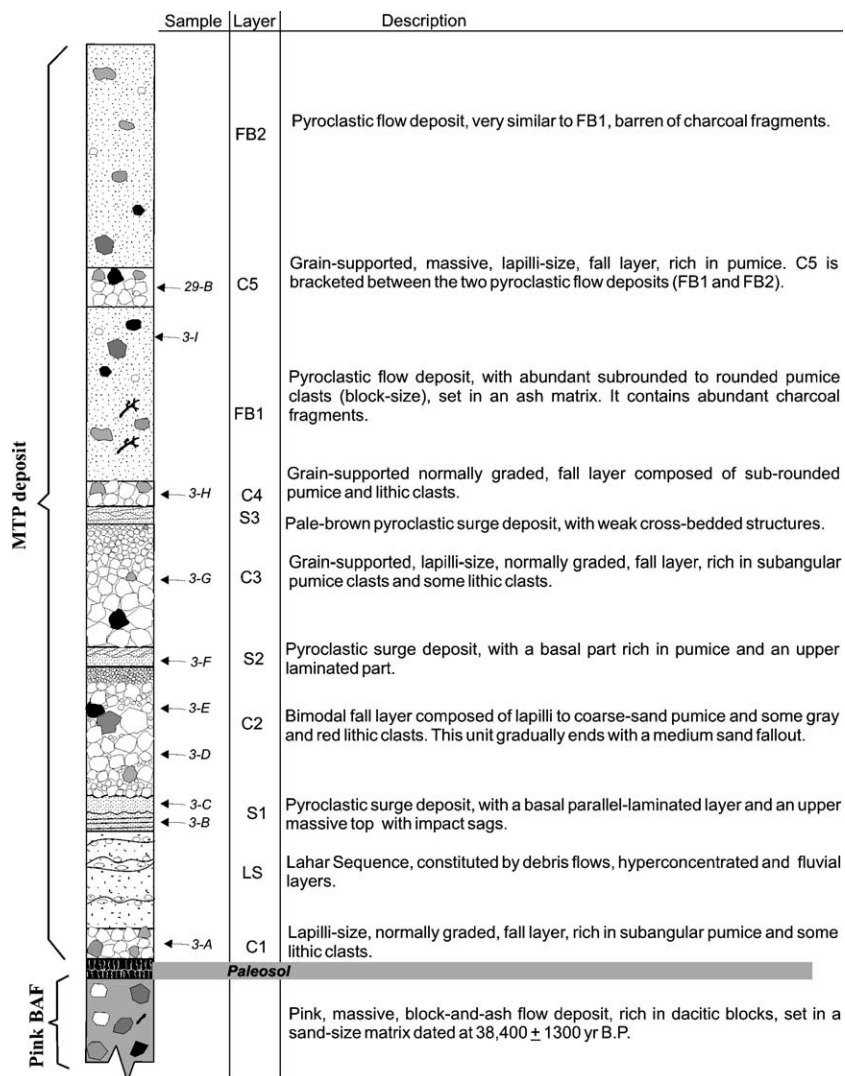


Fig. 3. Composite stratigraphic section of the MTP sequence and selected samples. An old pink block-and-ash flow deposit is also shown (BAF). C=fall deposits; LS=lahar sequence; S=surge deposit; FB=pyroclastic flow deposit. Thickness not to scale.

on top of a block-and-ash flow deposit dated at $38,400 \pm 1300$ years BP (Fig. 3). C1 is a pale gray, grain-supported, normally graded layer, up to 35 cm thick. It consists mainly of lapilli of pumice (65 vol.%), lapilli of red lithics (14 vol.%), glass (12 vol.%), and also crystal fragments (9 vol.%). At site 3, the deposit consists of coarse lapilli ($Md_{\phi} = -1.9$) and is moderately sorted ($\sigma_{\phi} = 1.7$) (Fig. 6). The maximum diameter of pumice clasts in the medial and upper parts is 12 cm. According

to the characteristics of this layer, it was classified as a fall deposit.

5. Lahar sequence (LS)

The LS consists of an alternating series of debris flow and fluvial layers that, at site 14, total 5.5 m (Fig. 7A). Individual layers range in thickness from 9.5 to 42 cm (Fig. 7B). This sequence is best exposed near

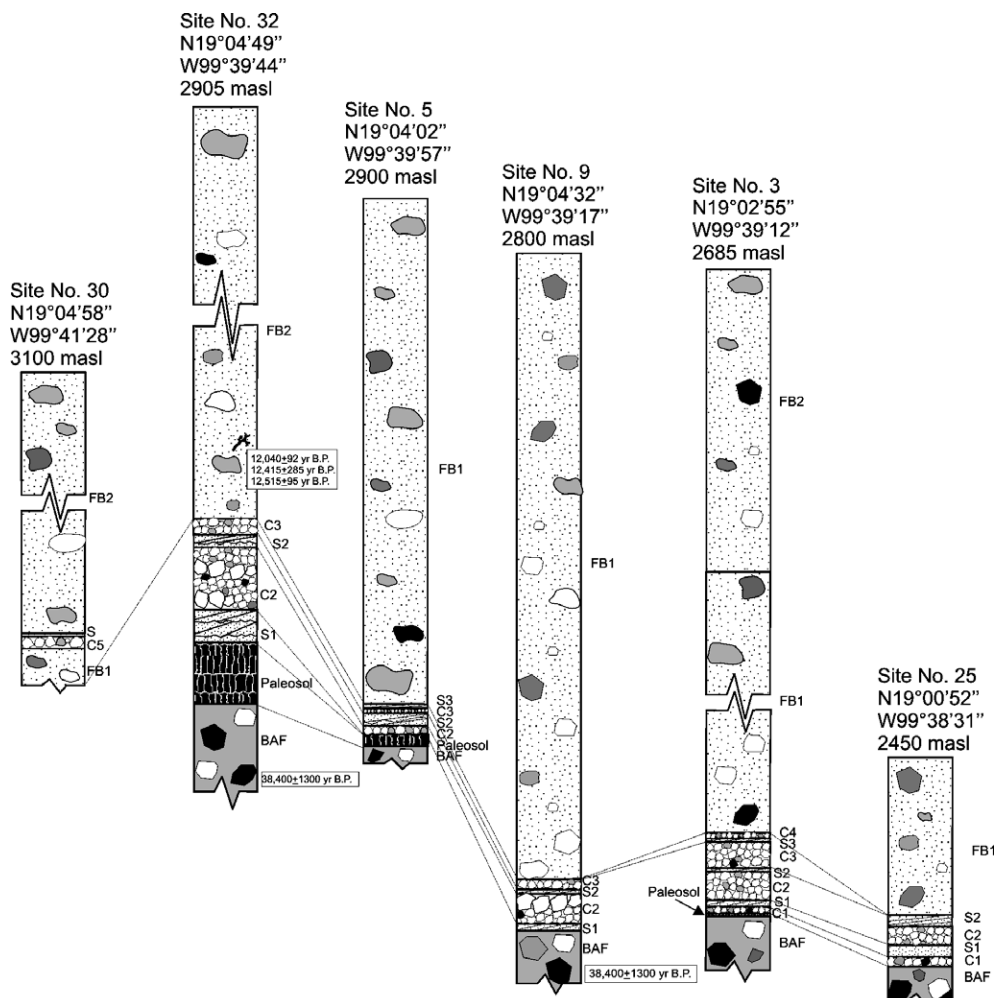


Fig. 4. Stratigraphic correlation of selected sections of the MTP deposits; the locations are shown in Fig. 2. The symbols are the same as in Fig. 3.

Tlanixco village (Fig. 2). At site 14, LS rests on an indurated lahar deposit of unknown age. The LS is composed of rounded pumice fragments, crystals, and lesser amounts of lithics, set in a medium to fine ash. Some layers show lenses of pumice, cross-bedding, and laminae. At site 14, LS has a median diameter of -1.5ϕ and is poorly sorted ($\sigma_\phi = 2.9$).

6. Layer S1

S1 overlies C1 with an erosional contact (Fig. 5). S1 is a pale gray to pink horizon, up to 25 cm

thick. It consists of a planar-laminated base and a massive upper part (Fig. 8A). The basal part consists of rounded pumice clasts (19%) and subangular lithics (30%) of coarse ash, supported by a fine ash matrix composed of glass shards (49%) and crystals (2%). The upper massive part is composed of lithics (29%) and pumice (34%), varying in size from 1.5 to 0.5 cm, respectively, supported by a fine ash matrix of glass shards (35%) and crystals (2%). At some sections (e.g., 73), deformation structures related to impact sags were found on top of this horizon (Fig. 8A). We classified S1 as a pyroclastic surge deposit, which has two distinctive

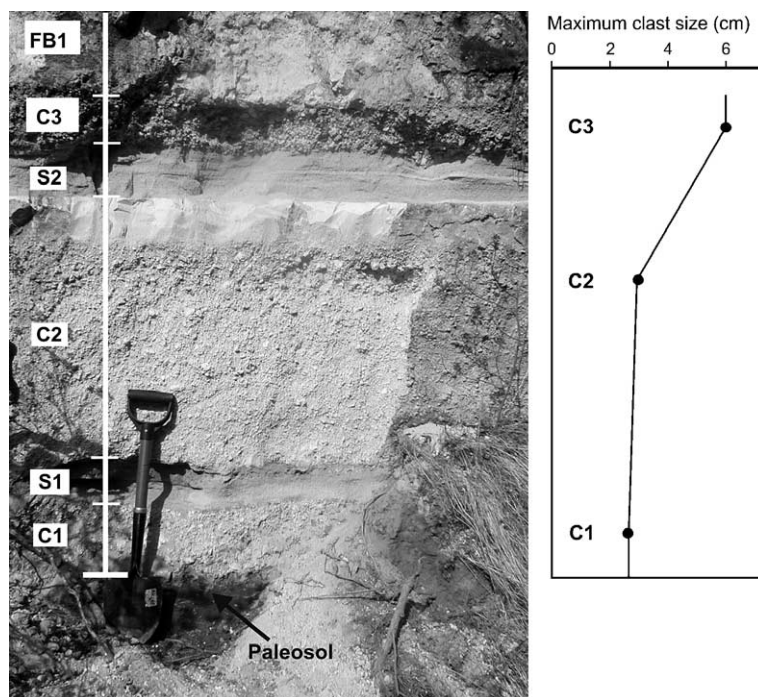


Fig. 5. Photograph of the MTP sequence at site 73, showing the stratigraphic relations between layers. The maximum lithic clast size is the average of five measurements. The shovel is 70 cm long.

granulometric distributions (Fig. 6). At site 73, the laminated base (sample 3B) has an Md_{ϕ} of 1.2 and is well sorted ($\sigma_{\phi}=0.5$), whereas the massive upper part is coarser ($Md_{\phi}=3.8$) but also well sorted ($\sigma_{\phi}=0.9$).

7. Layer C2

Layer C2 is grain-supported with asymmetric grading (reverse to normal) (Fig. 5). The maximum thickness of C2 is 97 cm where it contains block-size clasts. C2 represents the thickest fall layer of the MTP sequence. This horizon consists of angular lapilli and blocks of pumice (55%), up to 12 cm in diameter, and glass shards (21%), crystals (19%), and lithics (5%) of up to 5 cm in diameter. Ash aggregates with irregular shapes were found in this deposit during sieving. Most lithics occur in the middle part of the layer. They are gray porphyritic dacites with angular shapes, and internally show flow-banding structures and hydrothermal alteration. Typically, the uppermost part of C2 is

normally graded from medium to fine ash (Figs. 5 and 8B), containing pumice (49%), crystals (31%), glass shards (16%), and lithics (4%). The middle part of the deposit has an Md_{ϕ} of -1.5ϕ with poor sorting of $\sigma_{\phi}=2.5$ (Fig. 6), while the uppermost part (sample 3E) has an Md_{ϕ} of 1.8ϕ and is well sorted ($\sigma_{\phi}=0.8$).

8. Layer S2

Layer S2 locally eroded the top of layer C2 (Fig. 8B). It is pale gray, of irregular thickness with cross-bedding, and is composed of several layers. The basal part is rich in pumice fragments and is reversely graded, whereas the upper part is laminated. Layer S2, up to 30 cm thick, is composed of rounded pumice (43%) and subrounded lithics (12%), supported by a fine-ash matrix of crystals (38%) and glass shards (7%). At section 73, S2 shows impact sags at its top in contact with C3 (Fig. 5). At some localities, the laminated part exhibits cross-bedding at angles up to 13° with

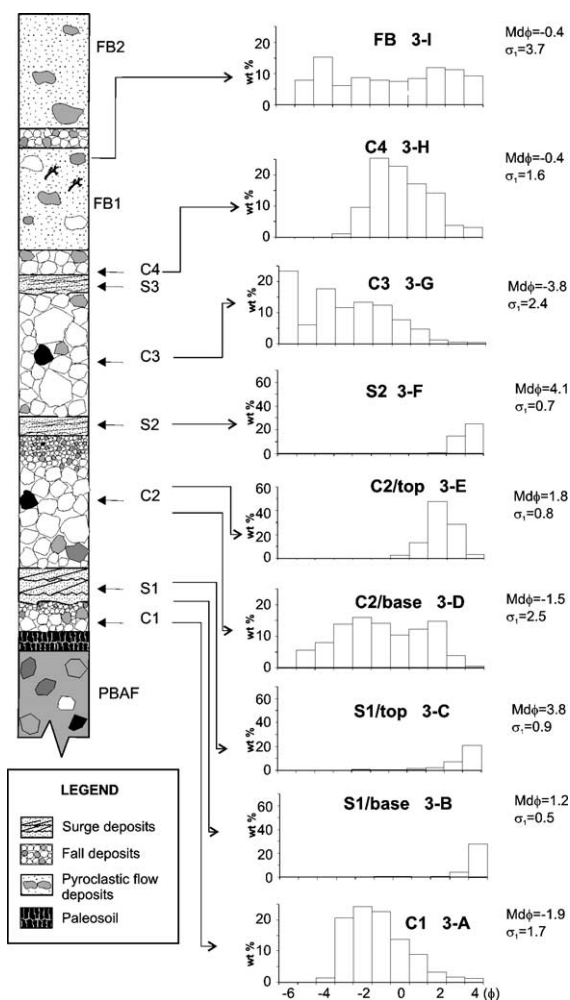


Fig. 6. Frequency histograms of the MTP sequence. Samples collected at section 3. Note the vertical variations of the sorting (σ_ϕ) and the median diameter (Md_ϕ).

respect to the enclosing bedding. At site 73, the base of S2 has an $Md_\phi=4.1$ and is well sorted ($\sigma_\phi=0.7$). S2 is a pyroclastic surge deposit.

9. Layer C3

Layer C3 overlies S2 along a flat planar contact (Figs. 5 and 8B). It is a pale gray, normally graded, grain-supported layer up to 55 cm thick. C3 is composed of pumice (55%), crystals (28%), lithics (11%), and glass shards (6%). The maximum diameter of pumice fragments is 6.5 cm, and

of lithics is 4.5 cm. The basal part of C3 contains some gray porphyritic angular lithics with cracks and hydrothermal alteration. The median grain-size diameter of this unit is -3.8ϕ , and it is poorly sorted ($\sigma_\phi=2.4$). We interpret this layer as a fall deposit.

10. Layer S3

Layer S3 erodes layer C3. It is pale brown, up to 5 cm thick, and has poorly developed cross-bedding (section 3). It is composed of fine ash particles of

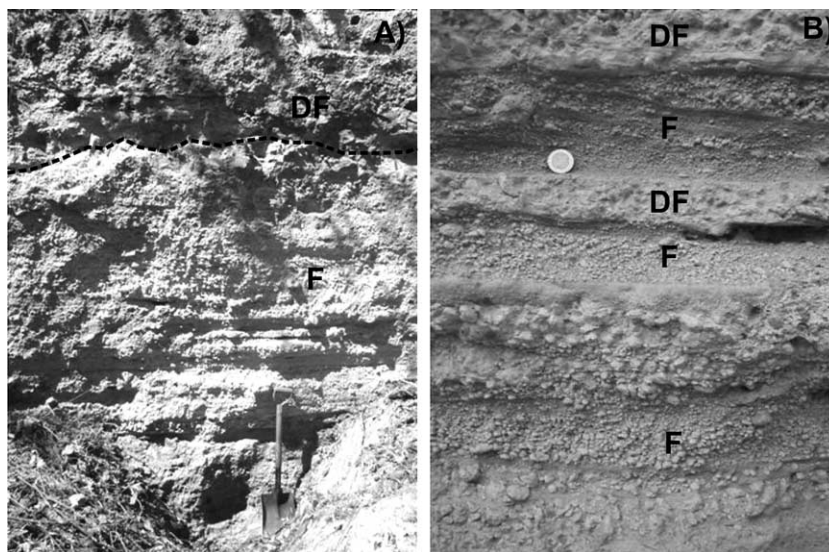


Fig. 7. (A) General view of the multilayered lahar sequence (LS) at site 12. The shovel is 1 m long. (B) Details of some layers of LS, which are composed of rounded pumice fragments. The coin is 1 cm in diameter. DF=debris flow deposits; F=fluvial deposit.

pumice, glass shards, crystals, and lithics. S3 is interpreted as a pyroclastic surge deposit.

11. Layer C4

Layer C4 is rarely exposed in the area. In the most complete outcrop, it rests conformably on S3 (Fig. 3). It is pale gray, grain-supported, and normally graded, and is composed of pumice (44%), lithics (14%), crystals (34%), and glass shards (4%). The maximum thickness is 8 cm, and the unit contains pumice and lithics up to 5 and 2.5 cm, respectively. The median

diameter is -0.4ϕ , and the unit has a moderate sorting ($\sigma_\phi = 1.6$) (Fig. 6). These features indicate a fall deposit.

12. Layers FB1, C5, and FB2

These deposits are distributed on the southeastern flank of the volcano. They overlie older deposits of Nevado de Toluca (Macías et al., 1997; García-Palomo et al., 2002), block-and-ash flow deposits, and all units of the MTP. These units are capped by a pale brown paleosol (section 46), debris flow

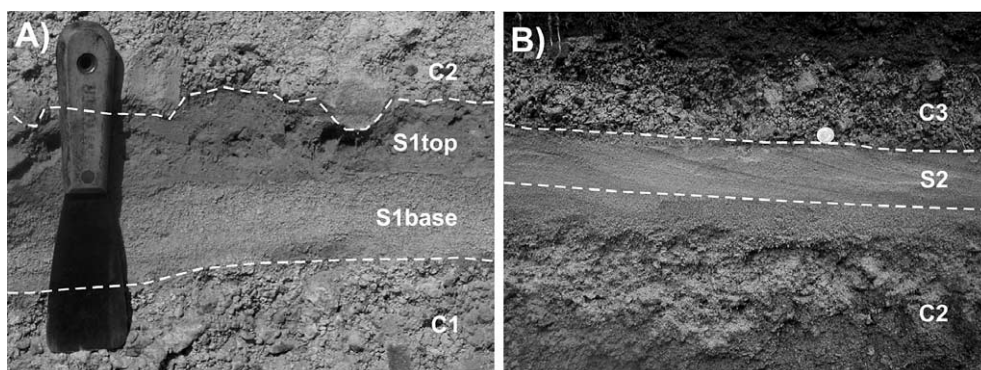


Fig. 8. (A and B) Photographs showing the characteristics of pyroclastic surge deposits (S1 and S2) at sites 26 and 9, respectively. C1, C2, and C3 are fallout layers. Note the impact sags on S1. The spatula is 15 cm and the coin is 4 cm in diameter.

deposits (site 65), and locally by the Upper Toluca Pumice.

FB1 and FB2 are both white, massive to sometimes slightly pink, pumice-rich pyroclastic flow units, with average thickness of 5 and 10 m, respectively. In the marginal portions of the deposits, they reach 85 cm in thickness, and are rich in fine particles (section 13). Locally, layers FB1 and FB2 display imbricated clasts, fumarolic pipes, and charred logs. The clasts are imbricated in a SE direction in the proximal facies (0–8 km from the summit) and to the S in the distal facies (8–14.5 km from the summit). Both units are composed of subrounded to rounded clasts of white and minor gray pumice (24%) up to 20 cm in diameter, juvenile lithics (31%) up to 15 cm, and accidental gray and red lithics (9%), all set in a medium to fine ash matrix composed of glass shards (7%) and crystals (29%). In two sections, these units are separated by a massive, pale gray, grain-supported fall layer (C5), which is up to 17 cm thick. At site 30, FB1 is poorly sorted ($\sigma_\phi=3.7$), with a median diameter of -0.4ϕ (Fig. 6). C5 appears only at site 30, where it is rich in pumice up to 10 cm in diameter and angular lithics up to 3 cm.

13. Density and vesicularity index

To identify possible variations in vesicularity that occurred during the MTP eruptive event, we carried out vesicularity measurements of pumice. Vesicularity depends on the volatile content, viscosity, eruption rate, and magma–water interactions (Sparks, 1978; Houghton and Wilson, 1989; Gardner et al., 1995). The density was measured in vesiculated fragments between 8 and 32 mm in diameter from C1, C2, C3, and FB1 deposits, following the techniques of Gardner et al. (1996) and Houghton and Wilson (1989). Using these density measurements, we also derived a vesicularity index throughout the MTP deposit. The results indicate that pumice density fluctuates in the fall horizons from 700 to 800 kg/m³, and is up to 890 kg/m³ in the pyroclastic flow deposit (Fig. 9). No major differences were found in the vesicularity index between the fallout horizons (C1, C2, and C3; 70–73 vol.%) and FB1, which averages 65 vol.%. These values agree with those published in previous works for magmatic fragmentation (Sparks, 1978;

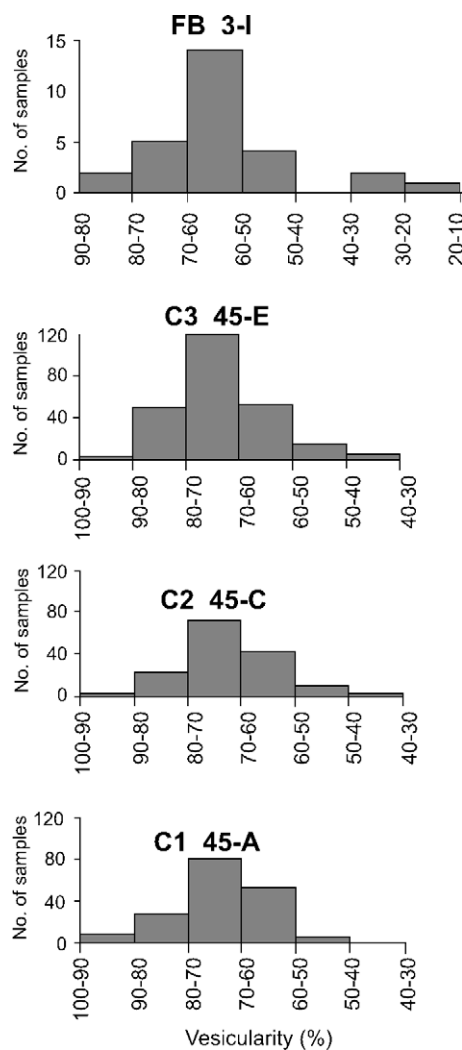


Fig. 9. Histograms of the vesicularity for some MTP horizons, sampled at site 45. Note that the vesicularity is homogeneous in all horizons analyzed.

Gardner et al., 1995). We also determined the density of some dense lithic clasts taken from several horizons, which averaged 2340 kg/m³, equivalent to a vesicularity of 6.4–10.4%.

14. Distribution and volume

The distribution of the MTP fall horizons was reconstructed from 71 stratigraphic sections. Thick-

ness and maximum lithic clasts were measured at each site. As the MTP deposit was extensively eroded and concealed by younger deposits (UTP), we were only able to reconstruct isopach and isopleth maps for layers C1 and C2.

The dispersal axis for layer C1 lies S65°E of the volcano (Fig. 10A). The 15-cm-thick isopach covers an area of 41 km². The isopleth map of layer C1 resembles the isopach map and has a main dispersal axis of S60°E (Fig. 10B). Layer C2 has a main dispersal axis S62°E (Fig. 10C). The area covered by the 40-cm isopach is 66 km². The isopleth map also has a main dispersal axis oriented S65°E (Fig. 10D).

The volumes of C1 and C2 fall layers were calculated following the method of Pyle (1989, 1995), as modified by Fierstein and Nathenson (1992) and

Carey et al. (1995), assuming a theoretical slope for the missing distal material. For C1, we estimate a volume of 1.5 km³. Assuming an average tephra density of 1000 kg/m³, the volume is equivalent to 1.5×10^{12} kg. The dense rock equivalent (DRE) volume is 0.6 km³, assuming a magma density of 2500 kg/m³. For C2, a total volume of 2.4 km³ was calculated, a mass of 2.4×10^{12} kg, and a DRE volume of 1 km³, using the same parameter values as for C1.

15. Pyroclastic surge and flow deposits

The pyroclastic surge deposits (S1, S2, and S3) are exposed on the SSE slopes of Nevado de Toluca and cover areas of 71, 55, and 35 km²,

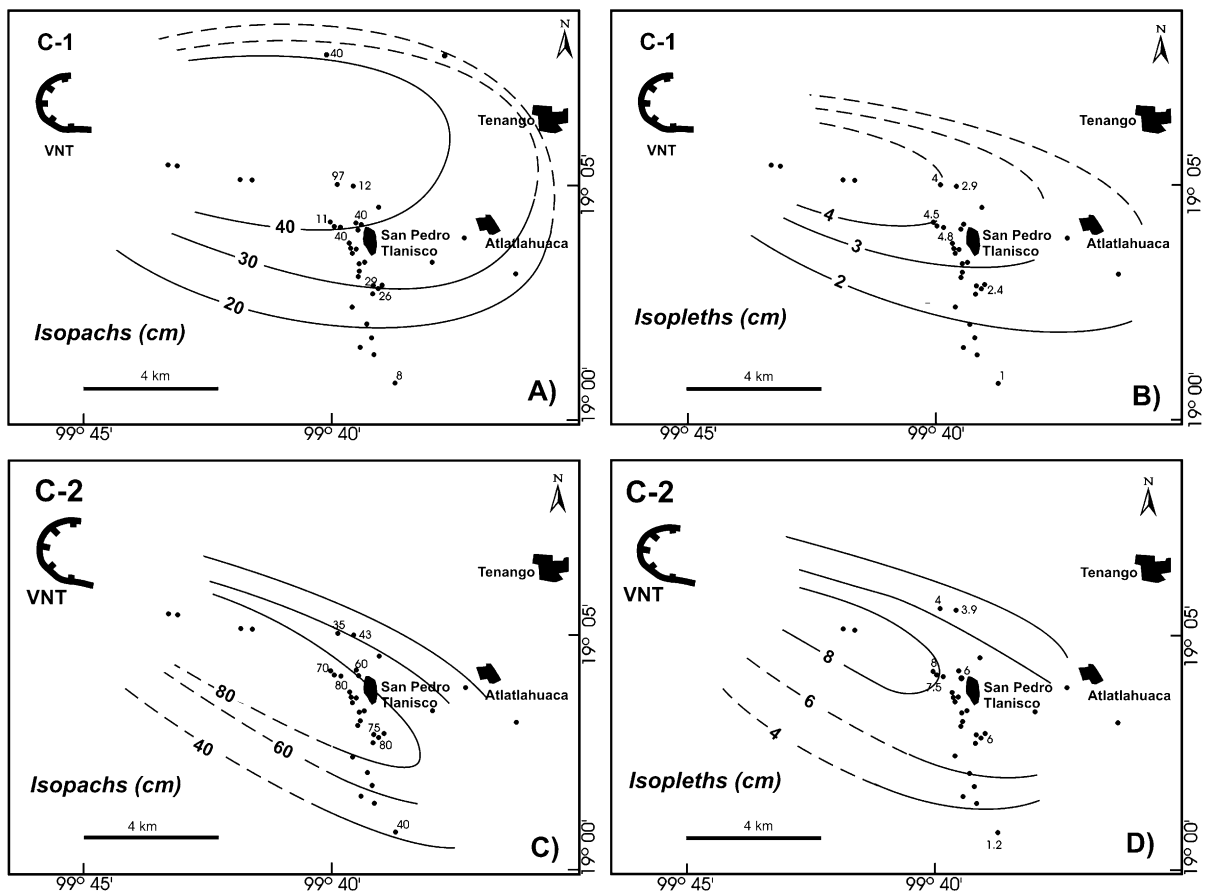


Fig. 10. Isopach and isopleth maps of layers C1 and C2 fall deposits of the MTP sequence. C1 (A and B) and C2 (C and D).

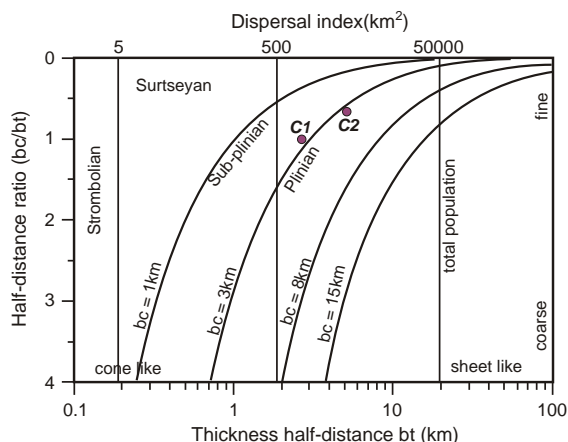


Fig. 11. Bt vs. bc/bt diagram (Pyle, 1989) used to classify the eruptive style of layers C1 and C2 fall deposits of the MTP sequence.

respectively. The pyroclastic flow deposits (FB1 and FB2) fill the Tlanixco, Cieneguilla, and Ciénega gullies that join downstream at Arroyo Grande gully. The distal ends of these deposits are located ~ 19 km from the volcano, near the villages of Villa Guerrero and Tenancingo de Degollado. The area covered by these deposits is 29 km^2 . Using an

average thickness of 14 m, the total tephra volume for the pyroclastic surges and flows is $\sim 0.41 \text{ km}^3$ (0.17 km^3 DRE). As we were unable to confidently estimate volumes for C3, C4, and C5, we assume that a minimum of 1.8 km^3 of magma was ejected during the MTP eruption. However, this volume is an underestimation because of the lack of enough MTP exposures.

16. Column heights

Based on the Pyle (1989) method, we determined bt and bc parameters for C1 and C2, which describe the grain-size characteristics for fallout deposits. These parameters were defined as the average distance over which the thickness (bt) and maximum lithic (bc) decrease by one half, and they can also be used to classify the eruptive style of the deposit. For C1 and C2, the values of bt were 2.5 and 4.9, and values of bc were 2.6 and 3.2, respectively. In general, bc values over 3 km indicate a Plinian eruptive style. Based on these values, C1 and C2 lie between subplinian and Plinian eruptions (Fig. 11). Assuming these horizons

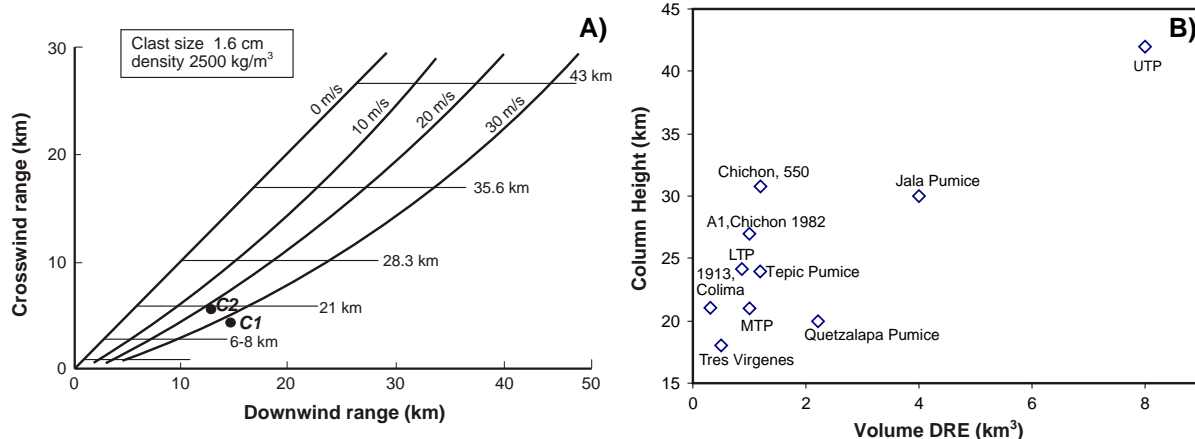


Fig. 12. (A) Downwind range vs. crosswind range isopleths from layers C1 and C2 used to calculate the column height (based on the Carey and Sparks, 1986 model). (B) DRE volume vs. column height of some Plinian eruptions in Mexico: the AD 1982 and 550 year BP events of El Chichón (Carey and Sigurdsson, 1986; Macías et al., 2003); the 1913 event of Volcán de Colima (Saucedo, 1997); the ~ 1000 year BP Jala Pumice of Ceboruco volcano (Gardner and Tait, 2000); the 6500 year BP La Virgen eruption of the Tres Virgenes Volcanic Complex (Capra et al., 1998); the $14,770 \pm 480$ year BP Tepic Pumice of Volcán San Juan, Nayarit (Lühr, 2000); and the $\sim 23,000$ year BP Quetzalapa Pumice eruption (Rodríguez-Elizarrarás et al., 2002), the LTP of 21,700 years BP (Capra et al., in press), the MTP of 12,100 years BP, and the 10,500 years BP UTP eruptions of Nevado de Toluca volcano (Arce et al., 2003). The latter is one of the largest eruptions reported to date.

formed from sustained subplinian to Plinian eruptions, we can use our lithic isopleth data with the model of Carey and Sparks (1986) to estimate plume heights of the eruptions. We obtained column heights of 19 km for C1 and 21 km for C2 (Fig. 12A). Mass eruption rate (MER) for the eruptive columns was calculated using the model of Sparks (1986). For C1, the MER was estimated at 2×10^7 kg/s and for C2 at 3×10^7 kg/s. The DRE volumes and column heights of the MTP eruptions are comparable to other Plinian eruptions that occurred in Mexico (Fig. 12B), such as the 1913 eruption of Colima volcano (Saucedo, 1997), or the eruption that deposited the Tepic Pumice (Luhr, 2000), but they are lower than the magnitude of the UTP eruption (Arce et al., 2003).

17. Analytical methods

In order to determine the chemical and mineralogical characteristics of the juvenile products as well as the pre-eruptive conditions of the magma, nine whole-rock analyses of pumice clasts were performed. Three of them were performed for major and trace elements by the ICP-MS method at Activation Laboratories (Ontario, Canada). The rest were analyzed for major and trace elements at the Geochemistry Laboratory of the Geological Institute at UNAM, Mexico, using the XRF method.

Modal analyses were performed on three pumice samples (Table 2) by using an automated point counter and a petrographic microscope. For each sample, we counted about 1000 points, using the

categories of plagioclase, orthopyroxene, hornblende, biotite, Fe–Ti oxides crystals, vesicles, and groundmass (microlites+glass).

Mineral and glass analyses were performed on the JEOL JXA-8600 electron microprobe at the CNR-Università di Firenze (Florence, Italy), using the following conditions: acceleration potential=15 kV; beam current=15 nA; and counting time 15–20 s. Glass analyses were conducted with a defocused beam of 10–15 μm in diameter, whereas a focused beam was used for mineral analyses. The data were corrected for matrix effects using the method of Bence and Albee (1968).

18. Petrography and mineralogy

Twelve polished sections of white, gray pumice and dense lithic clasts were examined under the petrographic microscope. All samples are porphyritic, with phenocrysts ranging in size from 0.3 mm to 3.3 mm (Fig. 13). Large phenocrysts commonly show signs of instability (e.g., anhedral forms, resorbed rims), whereas the smaller phenocrysts are euhedral. The total crystal content varies from 13 to 21 vol.%.

Plagioclase is the most abundant phase (9–14 vol.%), and is present as small crystals (<0.3 mm) as well as large phenocrysts (1.6 mm, rarely >3.3 mm). The phenocrysts show resorbed rims, with subhedral to anhedral forms, whereas small crystals (<0.3 mm) have euhedral forms. The plagioclase varies in composition from labradorite to andesine (Table 3). Chemical analysis of plagioclase resulted in minor anorthite variations in cores $\text{An}_{44.1 \pm 4.7}$ to $\text{An}_{47.4 \pm 4.3}$, and rims $\text{An}_{45.4 \pm 1.8}$ to $\text{An}_{45.7 \pm 3.2}$. Some phenocrysts show weak normal, reverse, or oscillatory zoning.

Orthopyroxene (Opx) is the second most abundant phase (2–5 vol.%). The crystals range in size from 0.2 to 0.9 mm. The enstatite content shows minor variations from En_{55} to En_{59} (Table 4). Hornblende (Hb) is also common, representing 0.7–1.6 vol.%, with crystal sizes varying from 0.2 to 0.9 mm. The chemical composition of Hb phenocrysts is uniform (Table 4) and falls within the edenite–hornblende group with Mg# varying from 41 to 58. Biotite represents up to 0.2 vol.% of the samples. Strikingly, single grains of

Table 2
Modal analysis of juvenile clasts of the deposit

Sample	Number	Plg of counts	Opx	Hb	Bt	Ox	Cum	Gmass	Ves
PBI-2A	1545	9.77	2.19	1.18	0.26	0.32	0.19	54.48	31.61
PBI-2B	1000	12.7	2.5	1.6	0.2	0.3	0.1	52.1	30.5
PBI29b	1000	14.5	4.9	0.7	0	0.3	1.2	47.8	30.6

Phenocrysts (>0.03 mm) vesicles, and groundmass (glass+microlites) were measured. Plg=plagioclase, Opx=orthopyroxene, Hb=hornblende, Bt=biotite, Ox=Fe–Ti oxides, Cum=clots of opx+hb+plg, Gmass=groundmass, Ves=vesicularity.

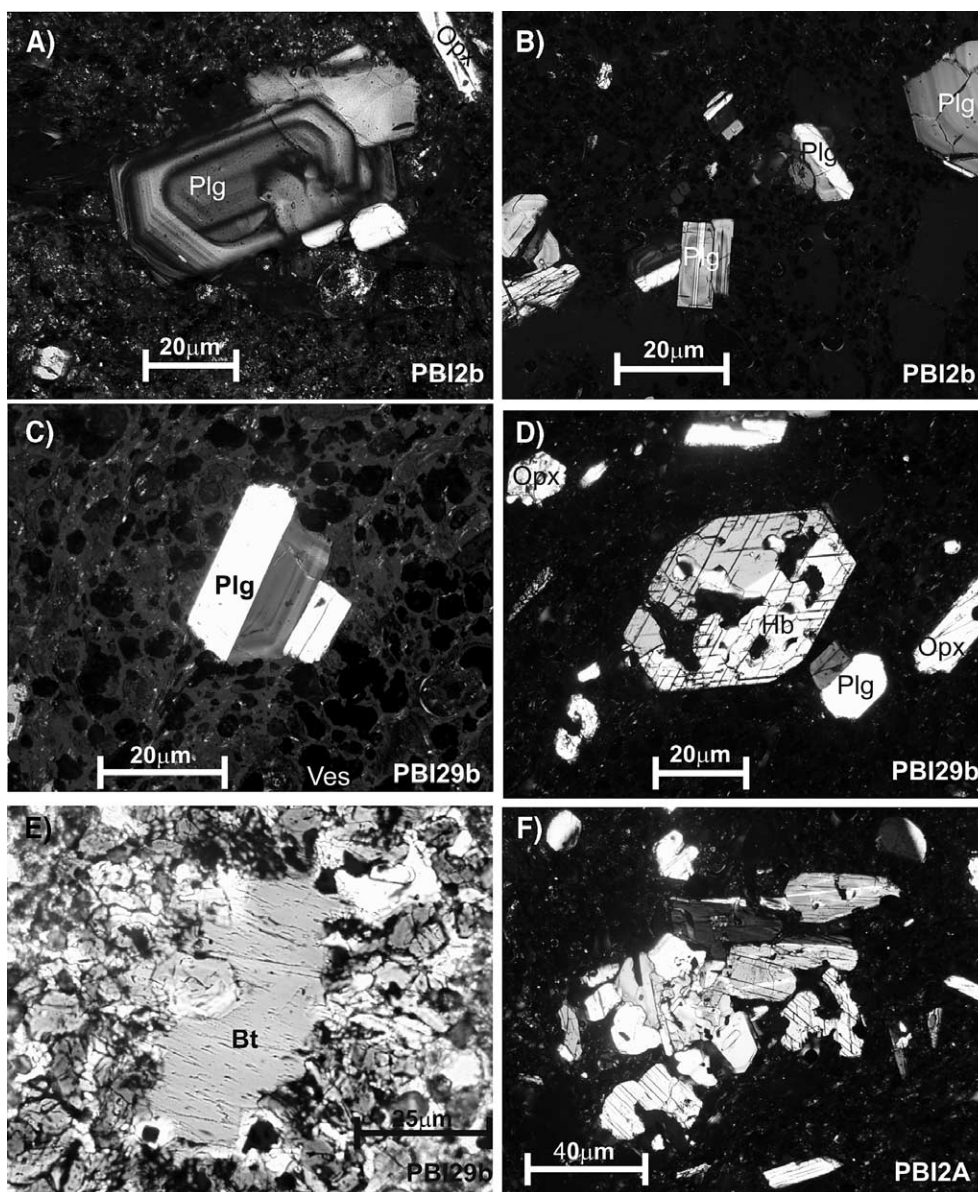


Fig. 13. Microphotographs of the MTP rocks: (A–C) stable crystals of plagioclase and orthopyroxene surrounded by groundmass and vesicles; (D) details of a hornblende crystal; (E) details of biotite xenocryst, showing the rim composed of orthopyroxene, hornblende, Fe–Ti oxides, and plagioclase; (F) example of crystal aggregates present in the MTP rocks. Plg=plagioclase; Hb=hornblende; Opx=orthopyroxene; Bt=biotite; Ves=vesicles.

biotite are an important constituent of the matrix of FB1. Biotite is usually large (up to 3 mm in length), and commonly has reaction rims (up to 0.5 mm wide) composed of orthopyroxene, hornblende, Fe–Ti oxides, and rare plagioclase. Biotite has a ferroan–phlogopite composition (Rieder et al., 1998; Table 4) with

Mg# varying from 45 to 47. According to Arce et al. (submitted for publication), biotite is xenocrystic in the MTP magma. Iron–titanium oxides are generally small, varying from 0.1 to 0.3 mm in diameter, and occur as isolated grains in the groundmass and in the rims of biotite phenocrysts. According to Arce et al.

Table 3
Selected plagioclase analyses of MTP samples

	SiO ₂	Al ₂ O ₃	FeO ^a	CaO	K ₂ O	Na ₂ O	Total	<i>n</i>
<i>Sample PBI 29B</i>								
c	56.06	28.03	0.23	9.75	0.23	5.82	100	8
r	56.49	27.77	0.32	9.42	0.26	6.09	100	11
Phenocryst 1								
r	54.58	29.31	0.25	10.68	0.20	5.30	100	
rc	58.61	26.57	0.21	7.60	0.33	6.63	100	
c	57.60	27.55	0.03	9.09	0.30	6.24	101	
c	56.44	28.13	0.00	9.11	0.31	5.99	100	
rc	57.98	27.26	0.16	8.66	0.28	6.39	101	
r	55.15	28.85	0.03	10.56	0.20	5.41	100	
<i>Sample PBI 2A</i>								
c	57.30	27.52	0.19	9.08	0.26	6.19	101	16
r	56.63	27.89	0.26	9.43	0.24	6.02	100	16
Phenocryst 2								
rr	56.32	28.05	0.25	9.16	0.26	6.39	100	
r	55.13	29.27	0.17	10.43	0.23	5.41	101	
rc	54.60	28.71	0.39	10.26	0.19	5.48	100	
c	55.48	29.10	0.19	10.61	0.17	5.53	101	
c	55.32	29.55	0.12	10.54	0.16	5.54	101	
rc	55.53	29.07	0.15	10.57	0.15	5.43	101	
r	55.49	28.49	0.10	10.55	0.17	5.54	100	
rr	58.36	27.09	0.22	8.36	0.26	6.73	101	

All data are reported as weight percent. c=core; r=rim; rc=mid-point between rim and core; rr=outermost rim. Values are average of *n* analyses. Two transects were made on two phenocrysts.

^a Total Fe as FeO.

(submitted for publication), ilmenite represents about 80 vol.% of the analyzed Fe–Ti oxide phases, and contains ilmenite molar fractions ranging from 0.89 to 0.87, and ulvöspinel molar fractions varying from 0.31 to 0.33. These authors calculated the crystallization temperature of the MTP magma by using the Fe–Ti oxide geothermometer of 817–840 °C and oxygen fugacities from –13.29 to –12.52. The groundmass consists of highly vesicular rhyolitic glass and minor amounts of microlites (essentially all plagioclase). The glass composition is very homogeneous (70–71 wt.% SiO₂) (Table 4).

19. Whole-rock composition

The juvenile products of the MTP deposit are composed of white, banded, and gray pumice clasts, as well as dense, gray lithic clasts. No compositional differences were found among the juvenile samples analyzed and reported in previous works (Arce et al., submitted for publication) and all lie within a narrow

dacitic composition of 63.2–65.4 SiO₂ wt.% (Fig. 14 and Table 5). The mineral assemblage and major and trace elements display minor variations, very similar to other deposits of Nevado de Toluca like the UTP (produced by a Plinian eruption) and BAF-13 (a block-and-ash flow deposit dated at ~13 ka) reported in Arce et al. (submitted for publication) (Fig. 14).

20. Discussion

20.1. Eruptive mechanisms

The MTP sequence lacks block-and-ash flow deposits that are produced by the partial or total destruction of domes, suggesting that the crater present at the top of the volcano was not plugged by a central dome. Instead, the restricted distribution of the pyroclastic flows of the MTP deposit on the ESE flanks of Nevado de Toluca suggests that the crater was already open to the east, as it is today. The reconstruction of the MTP stratigraphy suggests that the eruption occurred in five successive phases, hereafter referred to as Phases 1–5.

The eruption began with disruption of the solidified rock cap and the subsequent formation of an eruptive column that rose to a height of ~19 km

Table 4
Electron microprobe analyses of orthopyroxene, hornblende, biotite, and glass from MTP rocks

Mineral	Opx	Opx	Hb	Hb	Bt	Glass
Sample	29A	29B	29B	PBI-2A	PBI-29B	PBI-29B
<i>Oxides (wt.%)</i>						
SiO ₂	51.83	51.91	44.29	44.45	37.52	70.87
TiO ₂	0.07	0.17	2.22	1.79	4.09	0.19
Al ₂ O ₃	0.96	0.92	10.44	10.52	15.09	14.21
FeO ^a	24.28	24.29	14.25	14.51	16.40	2.05
MnO	0.59	0.68	0.25	0.19	0.13	nd
MgO	20.09	20.03	13.18	12.77	14.12	0.39
CaO	0.75	0.79	10.50	10.78	0.07	1.87
Na ₂ O	0.00	0.00	1.90	1.88	0.89	4.20
K ₂ O	0.04	0.02	0.39	0.48	7.59	2.71
Cr ₂ O ₃	0.02	0.02	0.02	0.07	0.02	nd
Total	98.61	98.8142	97.44	97.47	95.92	96.57
Mg#			48.36	46.81	46.26	
<i>n</i>	2	12	4	4	3	6

All values are averages of *n* analyses. Opx=orthopyroxene; Hb=hornblende; Bt=biotite. Mg number=100MgO/(MgO+FeO).

^a Total Fe reported as FeO.

Table 5
Whole-rock composition of MTP samples

Sample	29A-FBpz ^a	29C-int ^a	2A-C1 ^a	2B-C2 ^a	2C-C3 ^a	3H-C4 ^a	FB29Aw ^b	FB29Cg ^b	NT9545 ^c
SiO ₂	64.85	64.36	63.54	64.38	63.93	64.24	64.93	65.06	63.99
TiO ₂	0.64	0.66	0.64	0.64	0.64	0.6	0.64	0.64	0.58
Al ₂ O ₃	16.68	16.34	16.33	16.51	16.45	16.43	16.4	16.32	15.99
Fe ₂ O ₃	3.96	4.1	4.02	4.14	4.06	4.07	3.9	3.9	4.19
MnO	0.07	0.09	0.08	0.08	0.13	0.07	0.06	0.06	0.07
MgO	1.8	1.8	1.7	1.7	1.8	1.9	1.76	1.75	1.85
CaO	4.18	4.16	4.11	4.15	4.15	4.36	4.22	4.17	4.37
Na ₂ O	4.35	4.44	4.21	4.38	4.33	4.38	4.34	4.36	4.22
K ₂ O	1.98	1.98	1.96	1.97	1.94	1.88	1.89	2.05	1.93
P ₂ O ₅	0.17	0.17	0.18	0.18	0.17	0.15	0.19	0.19	0.58
LOI	1.61	1.96	2.53	2.39	2.46	2.02	1.77	1.38	2.27
Total	100.2	100.1	99.33	100.5	100	100.1	100.09	99.88	99.6
Ba							516	512	414
Rb	46	43	44	44	42	44	38	46	46
Sr	583	584	583	598	596	639	517	510	544
Y							12	12	14
Zr	181	182	180	180	180	154	141	138	115
Th	6	4	4	5	9	2	3	2.8	2.6
Pb							8	5	6
Zn	78	78	81	79	82	71	80	80	64
Cu							32	9	6
Ni	49	43	28	35	34	55	6	7	10
V							62	57	64
Cr							23.9	22.2	32.2
Hf							3.7	3.8	3.4
Cs							2	2.1	2
Sc							7.9	8	8.5
Ta							0.5	0.5	0.6
Co	68	61	37	48	46	71	13.9	8.4	8.2
Be							2	1	2
U							1.2	1.2	1.4
W							1	1	1
Mo							2	2	2
Au							2	2	2
La							16.7	16.8	13.3
Ce							34	35	31
Nd							18	16	11
Sm							3.6	3.5	3.2
Eu							1.12	1.14	1.01
Tb							0.3	0.3	0.5
Yb							1.12	1.13	1.34
Lu							0.18	0.17	0.18

Analyses of this study were performed at the Geochemistry Laboratory of the Geological Institute at UNAM, Mexico, by XRF method. Total Fe as Fe₂O₃. Major elements in weight percent (detection limits <0.01%), and trace elements in parts per million (detection limits: Sr, Y, Zr, Nb, Ga, Ni, and Cu <1; Rb and Cr, 2; Ba, 11; V, 5; Co, 3.

^a Data from this study.

^b Data from Arce et al. (2003).

^c Data from Macías et al. (1997).

(Phase 1). This pumice-rich Plinian column became richer with time in red hydrothermally altered lithics, suggesting that the volcanic conduit was

eroded. The eruptive column waned with time and the extreme normal grading of layer C1 suggests that the eruption ceased, allowing very fine ash to

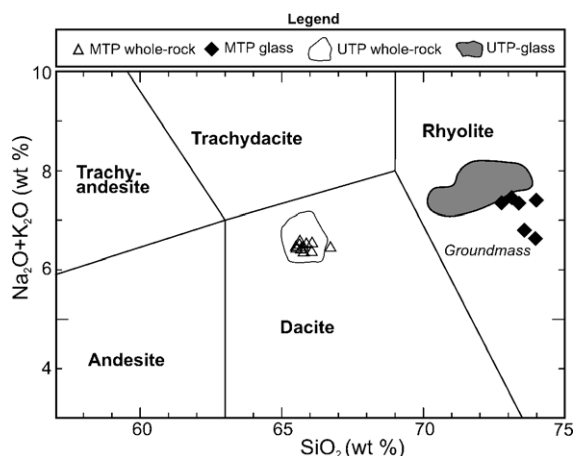


Fig. 14. Analyses of MTP rocks plotted on total alkalis vs. silica diagram (modified from Le Bas et al., 1986) for the classification of MTP rocks and glass. The UTP whole-rock and glass compositions are shown for comparison (Arce et al., submitted for publication). Note that the compositions of MTP and UTP are very similar.

settle out. During this time, rainfall mobilized loose pyroclastic materials of C1, generating lahars in the Arroyo Grande gully.

The eruption then reinitiated with a phreatomagmatic explosion that produced the S1 pyroclastic surge that traveled 16 km down the SE flanks of the volcano (Phase 2). It is possible that this event (S1) reopened the conduit, producing a subplinian column that rose 21 km above the crater and deposited layer C2. The asymmetric grading of the deposit indicates that, first, the energy of the eruption increased with time, eroding the conduit, as is shown by the presence of red altered lithics, and then energy waned gradually. The bimodal distribution of C2 and the presence of ash aggregates indicate the presence of moisture inside the eruptive column, provoking the accretion of fine particles and their premature fallout (Brazier et al., 1983; Sparks et al., 1981; Jurado-Chichay and Walker, 2001).

The eruption then continued as a series of hydro-magmatic explosions that generated a pyroclastic surge (S2) that flowed down the eastern flank of the volcano (Phase 3). Afterwards, a new eruptive column was established, dispersing fallout deposit C3 to the SSE. The energy of the flow disrupted parts of the conduit and deposited a large amount of red altered lithics (31 vol.%) until the eruption waned.

Almost immediately, a new magmatic explosion generated pyroclastic density currents (S3) and allowed the development of an eruptive column that was dispersed SE of the crater and deposited fallout layer C4 (Phase 4). The MER of the MTP eruption increased with time, as recorded in the sizes of lithics in the fall deposits (Fig. 5), after which the column collapsed (Phase 5), forming two pumice-rich pyroclastic flows. We do not have unequivocal data to explain this collapse; however, the decrease in the water content of the magma or the increase of MER by eroding the conduit could have been some causes to drive the eruption column to collapse as has been stated elsewhere (e.g., Wilson et al., 1980; Sparks et al., 1997). These flows were channeled along the Ciénega and Cieneguilla gullies for about 5 km, where they passed diverse obstacles, such as the Tepehuisco hill, and a hill made of older block-and-ash flow deposits (site 69). At the head of Arroyo Grande, the flows followed the gully. About 2 km to the north of San Pedro Tlanixco, the gullies merge into the Arroyo Grande, which drains to the south of the volcano. Here, the flows encountered the valley walls, they turned southwards and only the dilute upper parts reached the tops of topographic highs (site 55), leaving pumice and ash layers not thicker than 25 cm. The flows then traveled a further 8 km to the area today occupied by Villa Guerrero.

As described above, the MTP had a different evolution pattern compared with the other two Plinian eruptions at Nevado de Toluca (LTP and UTP). The 21.7 ka LTP eruption started with a magmatic explosion that generated a Plinian column and ended with phreatomagmatic activity that led to subplinian eruptive columns without column collapse (Capra et al., in press). The 10.5 ka UTP eruption, the biggest Plinian-type eruption occurring at Nevado de Toluca, started with phreatomagmatic activity followed by magmatic explosions, which developed high eruptive columns interrupted by several column collapse events (Arce et al., 2003). The MTP eruption recorded alternating magmatic and phreatomagmatic activity that ended with the collapse of the eruptive column. So, it is clear that phreatomagmatic activity has played an important role in the evolution of explosive activity at Nevado de Toluca volcano.

21. Origin of the MTP magma

Pre-eruptive conditions have been determined by Arce et al. (submitted for publication), who established that the MTP magma was stored at a temperature of 830 ± 13 °C at an f_{O_2} of -12.8 ± 0.52 . The magma stagnated below the volcano at a depth of ~ 4.5 – 6 km at water pressures between 150 and 200 MPa (Arce et al., submitted for publication). Under these conditions, the magma contained a mineral assemblage of plagioclase > hornblende > orthopyroxene > ilmenite > titanomagnetite > apatite plus xenocrysts of biotite embedded in a rhyolitic groundmass (70–71 wt.% in SiO₂).

The conditions mentioned above are inconsistent with the presence of a population of phenocrysts (pl, opx, hb, and Fe–Ti oxides) that have clear signs of disequilibrium (gulls, reaction rims, and dissolution borders). These resorption features suggest that the phenocrysts might also represent xenocrysts, like the biotite, from the host rock where the MTP magma resided, or that they underwent reheating by a hotter batch of magma. Perhaps this batch of hotter magma was not large enough to mix with the magma body residing below the volcano, and only provoked the reheating of the magmatic system.

22. Conclusions

Some 12,100 years BP, a Plinian–subplinian eruption took place at Nevado de Toluca volcano, here named the Middle Toluca Pumice (MTP). The eruption may have been caused by an injection of a mafic magma with the magma chamber that overturned the magmatic system. This caused an overpressure in a dacitic magma and eventually triggered the MTP eruption, generating at least 1.4 km^3 DRE of fragmental deposits. The juvenile products of the MTP have a dacitic composition (63–65 wt.% in SiO₂), with a mineral association composed of plagioclase, hornblende, orthopyroxene, titanomagnetite, ilmenite, and xenocrysts of biotite, all set in a rhyolitic groundmass (70–71% in SiO₂). The stratigraphic reconstruction of the eruption suggests that the event occurred in five eruptive phases, three of which generated Plinian–subplinian eruptive columns, and the other two of which produced pumiceous pyroclastic flows. Vesicu-

larity of the pumice clasts of the fall layers indicates that the eruption was dominated by magmatic explosions with minor hydromagmatic activity, which generated pyroclastic surges.

Acknowledgments

This work was supported by CONACYT grants (27993-T to J.L. Macías and 32312-T to J.M. Espíndola). We acknowledge the support received from E.A. González, J.T. Vázquez, and D.A. Aparicio from the Instituto de Geología, UNAM, during laboratory work and sample processing. We are indebted with R. Lozano, who performed seven chemical analyses of the samples at the X-ray fluorescence laboratory, and to M. Reyes, for her support during the SEM analysis. Fruitful discussions with L. Vázquez, T. Scolamacchia, K.M. Scott, and L. Capra enhanced our knowledge of this eruption. We are indebted to M. Branney, J. Gardner, M. Bursik, J.D. Keppie, B. Marsh (editor), and two anonymous reviewers who improved the ideas stated in this paper.

References

- Arce, J.L., Macías, J.L., Vázquez-Selem, L., 2003. The 10.5 ka Plinian eruption of Nevado de Toluca volcano, Mexico: stratigraphy and hazard implications. *Geol. Soc. Am. Bull.* 115, 230–248.
- Arce, J.L., Macías, J.L., Gardner, J.E., Layer, P.W., submitted for publication. Petrologic, ⁴⁰Ar–³⁹Ar, and experimental constraints on the Nevado de Toluca magma chamber, Mexico, Around 10.5 ka. *J. Petrol.*
- Bence, A.E., Albee, A.L., 1968. Empirical correction factors for the electron microanalysis of silicates and oxides. *J. Geol.* 76, 382–403.
- Bloomfield, K., Valastro, S., 1974. Late Pleistocene eruptive history of Nevado de Toluca volcano, Central Mexico. *Geol. Soc. Am. Bull.* 85, 901–906.
- Bloomfield, K., Valastro, S., 1977. Late Quaternary tephrochronology of Nevado de Toluca volcano, central Mexico. *Overseas Geol. Miner. Resour.* 46, 1–15.
- Bloomfield, K., Sánchez-Rubio, G., Wilson, L., 1977. Plinian eruptions of Nevado de Toluca. *Geol. Rundsch.* 66, 120–146.
- Brazier, S., Sparks, R.S.J., Carey, S.N., Sigurdsson, H., Westgate, J.A., 1983. Bimodal grain size distribution and secondary thickening in air-fall ash layers. *Nature* 301, 115–119.
- Bursik, M., 1993. Subplinian eruption mechanisms inferred from volatile and clast dispersal data. *J. Volcanol. Geotherm. Res.* 57, 47–60.

- Capra, L., Macías, J.L., Espíndola, J.M., Siebe, C., 1998. Holocene Plinian eruption of La Virgen volcano, Baja California, Mexico. *J. Volcanol. Geotherm. Res.* 80, 239–266.
- Capra, L., Carreras, L., Arce, J.L., Macías, J.L., in press. The Lower Toluca Pumice: A ~21,700 yr B.R. Plinian eruption at Nevado de Toluca volcano, Mexico. *Geol. Soc. Am. Bull.*
- Carey, S.N., Sigurdsson, H., 1986. The 1982 eruptions of El Chichón volcano, Mexico (2): Observations and numerical modeling of tephra fall distribution. *Bull. Volcanol.* 48, 127–141.
- Carey, S.N., Sparks, R.S.J., 1986. Quantitative models of fallout and dispersal of tephra from volcanic eruption columns. *Bull. Volcanol.* 48, 109–125.
- Carey, S.N., Gardner, J.E., Sigurdsson, H., 1995. The intensity and magnitude of Holocene Plinian eruptions from Mount St. Helens volcano. *J. Volcanol. Geotherm. Res.* 66, 185–202.
- Cervantes, K., 2001. La Pómez Blanca Intermedia: depósito producido por una erupción Pliniana–subpliniana del Volcán Nevado de Toluca hace 12,100 años. Master Thesis, UNAM, México, DF, 86 pp.
- Cioni, R., Marianelli, P., Santacroce, R., Sbrana, A., 2000. Plinian and Subplinian eruptions. In: Sigurdsson, H. (Ed.), *Encyclopedia of Volcanoes*. Academic Press, pp. 477–494.
- Cioni, R., Sulpizio, R., Garruccio, N., 2003. Variability of the eruption dynamics during a subplinian event: the Greenish Pumice eruption of Somma–Vesuvius (Italy). *J. Volcanol. Geotherm. Res.* 124, 89–114.
- Fierstein, J., Nathenson, M., 1992. Another look at the calculation of fallout tephra volumes. *Bull. Volcanol.* 54, 156–167.
- García-Palomo, A., Macías, J.L., Arce, J.L., Capra, L., Garduño, V.H., Espíndola, J.M., 2002. Geology of Nevado de Toluca volcano and surrounding areas, central Mexico. *Geol. Soc. Am. Map Series*. 1–48 pp.
- Gardner, J.E., Tait, S., 2000. The caldera-forming eruption at Volcán Ceboruco, Mexico. *Bull. Volcanol.* 62, 20–33.
- Gardner, J.E., Rutherford, M., Carey, S., Sigurdsson, H., 1995. Experimental constraints on pre-eruptive water contents and changing magma storage prior to explosive eruptions of Mount St Helens volcano. *Bull. Volcanol.* 57, 1–17.
- Gardner, J.E., Thomas, R.M.E., Jaupart, C., 1996. Fragmentation of magma during Plinian volcanic eruptions. *Bull. Volcanol.* 58, 144–162.
- Houghton, B.F., Wilson, C.J.N., 1989. A vesicularity index for pyroclastic deposits. *Bull. Volcanol.* 51, 451–462.
- INEGI, 1995. Censo 95 de Población y vivienda: Resultados definitivos. *Tabuladores básicos (Estados de México (551 pp.))*.
- Inman, D.L., 1952. Measures for describing the size distribution of sediments. *J. Sediment. Petrol.* 22, 125–145.
- Jurado-Chichay, Z., Walker, G.P.L., 2001. Variability of plinian fall deposits: examples from Okataina Volcanic Centre, New Zealand. *J. Volcanol. Geotherm. Res.* 111, 239–263.
- Le Bas, M.J., Le Maitre, R.W., Streckaisen, A., Zanettin, B., 1986. A chemical classification of volcanic rocks based on the total alkali–silica diagram. *J. Petrol.* 27, 745–750.
- Luhr, J., 2000. The geology and petrology of Volcán San Juan (Nayarit, México) and the compositionally zoned Tepic Pumice. *J. Volcanol. Geotherm. Res.* 95, 109–156.
- Macías, J.L., García-Palomo, A., Arce, J.L., Siebe, C., Espíndola, J.M., Komorowski, J.C., Scott, K.M., 1997. Late Pleistocene–Holocene cataclysmic eruptions at Nevado de Toluca and Jocotitlán volcanoes, Central Mexico. In: Kowallis, B.J. (Ed.), *Proterozoic to Recent Stratigraphy, Tectonics, and Volcanology, Utah, Nevada, Southern Idaho and Central Mexico*. *BYU Geology Studies*, pp. 493–528.
- Macías, J.L., Arce, J.L., Mora, J.C., Espíndola, J.M., Saucedo, R., Manetti, P., 2003. A 550-year-old Plinian eruption at El Chichón volcano, Chiapas, Mexico: explosive volcanism linked to reheating of the magma reservoir. *J. Geophys. Res.* 108 (B12), 2569.
- Newton, A.J., Metcalfe, S.E., 1999. Tephrochronology of the Toluca Basin, central Mexico. *Quat. Sci. Rev.* 18, 1039–1059.
- Pyle, D.M., 1989. The thickness, volume and grain size of tephra fall deposits. *Bull. Volcanol.* 51, 1–15.
- Pyle, D.M., 1995. Assessment of the minimum volume of tephra fall deposits. *J. Volcanol. Geotherm. Res.* 69, 379–382.
- Rieder, M., Cavazzini, G., D'yakonov, Y.S., Frank-Kamenetskii, V.A., Gottardi, G., Guggenheim, S., Koval', P.V., Müller, G., Neiva, A.M.R., Radoslovich, E.W., Robert, J.L., Sassi, F.P., Takeda, H., Weiss, Z., Wones, D.R., 1998. Nomenclature of the Micas. *Can. Mineral.* 36, 1–48.
- Rodríguez-Elizarrarás, S.R., Siebe, C., Komorowski, J.C., Abrams, M., 2002. The Quetzalapa Pumice: a voluminous late Pleistocene rhyolite deposit in the eastern Trans-Mexican Volcanic Belt. *J. Volcanol. Geotherm. Res.* 113, 177–212.
- Saucedo, R., 1997. Reconstrucción de la erupción de 1913 del Volcán de Colima. Master Thesis, UNAM, México, DF, 127 pp.
- Sieh, K., Bursik, M., 1986. Most recent eruption of the Mono Craters, eastern central California. *J. Geophys. Res.* 91, 12539–12571.
- Sparks, R.S.J., 1978. The dynamics of bubble formation and growth in magmas: a review and analysis. *J. Volcanol. Geotherm. Res.* 3, 1–37.
- Sparks, R.S.J., 1986. The dimensions and dynamics of volcanic eruption columns. *Bull. Volcanol.* 48, 3–15.
- Sparks, R.S.J., Wilson, L., Sigurdsson, H., 1981. The pyroclastic deposits of the 1875 eruption of Askja. *Philos. Trans. R. Soc. Lond.* 229, 241–273.
- Sparks, R.S.J., Bursik, M.I., Carey, S.N., Gilbert, J.S., Glaze, L.S., Sigurdsson, H., Woods, A.W., 1997. *Volcanic Plumes*. John Wiley & Sons, New York. 560 pp.
- Stuiver, M., Reimer, J., 1993. Extended ¹⁴C data base and revised CALIB 4.1 ¹⁴C age calibration program. *Radiocarbon* 35, 215–230.
- Stuiver, M., Reimer, J., Bard, E., Beck, J.W., Burr, G.S., Hughen, K.A., Kromer, B., McCormac, G., Van der Plicht, J., Spurk, M., 1998. INTCAL98 radiocarbon age calibration, 24,000–0 cal BP. *Radiocarbon* 40, 1041–1083.
- Wilson, L., Sparks, R.S.J., Walker, G.P.L., 1980. Explosive volcanic eruptions IV. The control of magma properties and conduit geometry on eruption column behavior. *Geophys. J. R. Astron. Soc.* 63, 117–148.